Published version: *Inorganic Chemistry* 2023, 62, 16161-16169

Meltable Hybrid Antimony and Bismuth Iodide 1D Perovskites

Ethan J. Crace,[1] Akash Singh,[1,2] Stella Haley,[1] Bethany Claes,[3] David B. Mitzi[1,4*]

1. Department of Mechanical Engineering and Materials Science, Duke University, Durham, NC 27708, United States.
2. University program in Materials Science and Engineering, Duke University, Durham, North Carolina 27708, United States.
3. Department of Materials Science and Engineering, University of Tennessee Knoxville, Knoxville, Tennessee 37996, United States.
4. Department of Chemistry, Duke University, Durham, NC 27708, United States.

* david.mitzi@duke.edu

Abstract

Hybrid lead-halide perovskites have been studied extensively for their promising optoelectronic properties and prospective applications including photovoltaics, solid-state lighting, and radiation detection. Research into these materials has also been aided by the simple and low temperature synthetic conditions involved in solution-state deposition/crystallization or melt processing techniques. However, concern over lead toxicity has plagued the field since its early days. One of the most promising routes to mitigating toxicity in hybrid perovskite materials is substituting isoelectronic Bi(III) for Pb(II). Various methods have been developed to allow pnictide-based systems to capture properties of the Pb(II) analogs, but the ability to melt process extended hybrid pnictide-halide materials has not been investigated. In this work, we prepare a series of 1D antimony and bismuth-iodide hybrid materials employing tetramethylpiperazinium (TMPZ)-related cations. We observe, for the first time, the ability to melt hybrid pnictide-halide materials for both Sb(III) and Bi(III) systems. Additionally, we find that Sb(III) analogs melt at lower temperatures, and attribute this observation to structural changes induced by the increased stereochemical activity of the Sb(III) lone pair coupled with reduction in effective dimensionality due to steric interactions with the organic cations. Finally, we demonstrate the ability to melt process phase pure thin films of (S-MeTMPZ)SbI_5.

Introduction

Hybrid metal-halide perovskites have been established as promising materials for myriad applications including photovoltaics (PV),[1-4] solid-state lighting,[3-6] and radiation detection.[7-8] These materials, particularly the lead-halide perovskites, have been studied extensively due to their favorable properties and the ability to prepare single crystals, powders, and thin films from low temperature, solution processing methods.[6, 9-11] For device applications, the ability to process thin films via spin or blade coating provides a clear path to producing devices at scales compatible with commercialization. In addition to solution-based processing techniques, certain 2D germanium-, tin- and lead-halide perovskites also melt before decomposition of the organic templating cation, allowing the materials to be melt processed rather than requiring a solution.[12-21] Melt processing of perovskites provides another opportunity to scale up production of perovskite devices, eliminating the need for use of toxic solvents such as dimethylformamide (DMF) or dimethylsulfoxide (DMSO), and less waste is generated in the process of preparing the films. Beyond films, melting at temperatures significantly below the melting temperature affords opportunities for crystal growth[12, 21] and prospectively glass formation.[14, 22-23]

Most studies on hybrid perovskite device performance and processing have focused on the lead-halide-based systems, which contain toxic and water soluble Pb(II) cations. Considerable effort has been targeted toward replacing lead with its lighter analog tin;[24-25] however, the loss of relativistic effects that stabilize the valence *s* electrons in Pb(II) allows for facile oxidation of Sn(II) to Sn(IV) under ambient conditions. Another route to removing Pb(II) involves replacing the element with isoelectronic and non-toxic Bi(III) coupled with another non-toxic M(I) species. The resulting "double perovskites" (or elpasolites) have been studied as possible replacements for 3D and 2D lead perovskites as they show some similar properties and can still be solution processed under appropriate conditions.[26-27] In addition to replacing two Pb(II) cations with M(I) and Bi(III), certain organic cations can template formation of 2D perovskite layers that only contain Bi(III) or Sb(III) cations, with 1/3 of the layer metal sites vacant.[28] Further, 2D perovskites conceptually derived from <111>-oriented cuts of the 3D perovskite (as opposed to the more typical <100>-oriented cuts) can also form Bi or Sb perovskite layers with full metal occupancy and hold interest for PV and other applications.[29-31] However, for typical hybrid 2D perovskite syntheses, a direct substitution of SbI_3 or BiI_3 for SnI_2 or PbI_2 often leads to lower dimensional materials with the formula $(A^+)_2MI_5$ or $(A^{2+})MI_5$ (M = Sb or Bi), which can adopt a "1D perovskite" structure with zigzag corner-sharing chains of metal halide octahedra.[32-33] This drop in dimensionality is caused by the increased charge of the Sb(III) and Bi(III) centers, leading to the inclusion of an additional iodide anion for charge balance. The 1D pnictide perovskites are semiconductors and show excitonic properties,[32] which points to similar applications as for 2D perovskites, including non-linear optics[34-35] or radiation detection.[36]

While the replacement of Pb(II) or Sn(II) with Bi(III) or Sb(III) has shown promise, to our knowledge, no studies have examined the possibility of preparing such pnictide-based perovskites by melt processing. We therefore began studying the melting properties of 1D antimony and bismuth halide perovskites. Examination of purely inorganic binary metal halides suggests no clear melting point trends in transitioning between divalent and trivalent metal halides. For example, SnI_2 melts at 316 °C,[37] while SbI_3 melts at 170.5 °C.[37] Meanwhile, PbI_2 has a melting point of 400 °C,[37] while BiI_3 melts at 408.6 °C.[37] Melting temperature trends are expected to be a convolution of the increased ionic attraction afforded by the larger charge on the trivalent versus the divalent metal ions, coupled with differences in the detailed crystal structures (e.g., the more molecular or

0D structure of SbI_3 leads to an anomalously low melting point relative to the analogous values for the higher-dimensional SnI_2 or BiI_3 structures). Further, in hybrid systems, the supramolecular interactions among the organic moieties and hydrogen bonding interactions among organic and inorganic components are likely to play a significant role in determining melting temperature relative to the decomposition point. Therefore, the question of melting point in the Bi/Sb halide perovskite family represents an interesting and unexplored direction in the hybrid perovskite field.

We initially tested Bi analogs of Sn and Pb perovskites (same organic cation choice) that were previously demonstrated to melt. Specifically, we considered bismuth-iodide hybrids templated by rigid/bulky ammonium cations such as 2-naphthylethylammonium (NEA) or long chain alkylammonium cations like dodecanediammonium (DDDA).[13, 17] The latter compound has been previously reported[32] and consists of 1D bismuth-iodide chains. The former compound based on NEA was not reported. Single crystal x-ray diffraction data of the material determined the chemical formula as $(NEA)_3Bi_2I_9$, with a structure consisting of bismuth-iodide dimers similar to inorganic $A_3Bi_2I_9$ structures (Table S1).[38-39] Attempts to heat both of these materials above 270 °C on a hot plate only produced decomposition, observed as blackening and smoking of the crystals and powders—i.e., these compounds failed to melt, despite the bulky organic cations and lower structural dimensionality. We next explored other known 1D bismuth-iodide perovskites to look for a promising candidate with regards to melting characteristics. Among the examined materials, we found the perovskite $(TMPZ)BiI_5$ (where TMPZ = 1,1,4,4-tetramethylpiperazine), which interestingly has no strong N-H-I hydrogen bonding interactions because all ammonium moieties are quaternary, but will still have weaker hydrogen bonding interaction between the methyl and methylene groups (which are all adjacent to quaternary ammonium moieties).[40] After simple tests on a hot plate, we found that $(TMPZ)BiI_5$ melts before complete decomposition of the organic cations. Based on this discovery, we synthesized two novel Sb-I and an additional new Bi-I perovskite derived from $(TMPZ)BiI_5$ (Table S2). All three of these materials, $(TMPZ)SbI_5$, (S-MeTMPZ)SbI_5, and (S-MeTMPZ)BiI_5 (where S-MeTMPZ = (*S*)-1,1,2,4,4-pentamethylpiperazinium; the acronym is based on the alternative nomenclature (*S*)-2-methyl tetramethylpiperazinium to highlight the similarity of the compounds within the current study), show lower melting points than $(TMPZ)BiI_5$. In this work, we will highlight and compare the structural differences among these four materials, quantitatively measure their thermal properties, and demonstrate the ability to melt and recrystallize one of these materials, (S-MeTMPZ)SbI_5, while completely maintaining the original crystalline structure.

Structural Comparison

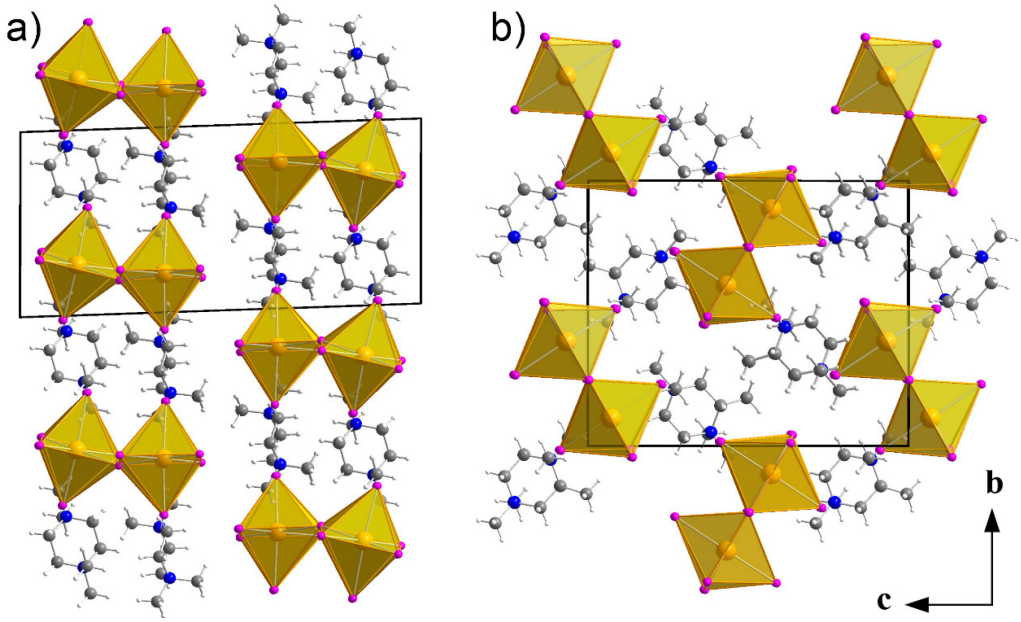

Figure 1. Comparison of (a) (TMPZ)BiI_5 and (b) (S-MeTMPZ)BiI_5 crystal structures. Black boxes indicate unit cell edges and both unit cells are oriented so that the *b*-axis is up and the *c*-axis is left and right as indicated by the axis label (bottom right)

The structure of (TMPZ)BiI_5 was fully described in the publication where it was first reported.[40] However, we will revisit the structure here, to provide consistent language for comparing the 1D pnictide-halide hybrid structures examined in this work and to draw clear connections to the trends in thermal properties. The compound crystallizes in the *P-1* space group as a 1D material with corner-sharing octahedra in a zig-zag pattern (Figure 1 and 2). Due to the low symmetry of the structure, there are two crystallographically unique bismuth atoms, which produce octahedra that possess different types of distortions from ideal octahedral geometry (Figure 2a). One of the octahedra can be nominally thought of as a square pyramid with a long contact to the final iodide anion (completing the distorted octahedral coordination). Taking this view, the iodide anions that form the base of the pyramid (hereafter basal) have intermediate bond lengths ranging from 2.95-3.25 Å. The longest of these bonds (3.25 Å) is between the bismuth cation and one of the μ iodides that connects the two unique bismuth atoms. The Bi-I bond trans to this longest basal bond is the shortest basal bond (2.95 Å). The overall shortest Bi-I bond length (2.92 Å) is terminal and forms the peak of the square pyramid. Trans to this bond is the long contact between the bismuth cation and the other μ iodide with the longest Bi-I bond distance in the crystal structure at 3.47 Å. This variance in bond length results in increased values for Δ_{oct} and λ_{oct}, which are distortion parameters that measure the difference of M-X bond lengths from their average value and the ratio of the M-X bond length to an idealized bond length for an ideal octahedron of the same volume, respectively (see SI for full definition).[41-42] Because Δ_{oct} is derived from a difference in value and λ_{oct} is based on ratios, values close to 0 for Δ_{oct} and 1 for λ_{oct} are considered less distorted. Additionally, λ_{oct} values below 1 indicate that the bonds tend to be shorter than the ideal values and values above 1 indicate they are longer. For this octahedron, $\Delta_{oct} = 3.61 \times 10^{-3}$ and $\lambda_{oct} = 0.984$. Despite the deviations in bond length, this octahedron is otherwise nominally undistorted, with *cis* I-Bi-I bond angles close to 90° and, consequently, a low value for the distortion parameter σ^2_{oct} of 7.58, which measures the difference between *cis* X-M-X bond angles from 90° (full

definition is given in the SI).[42] Similar to Δ_{oct}, values closer to 0 are less distorted because σ^2_{oct} is based on measuring a difference rather than a ratio.

The other unique octahedron has a smaller range of bond lengths (2.92-3.33 Å). The two Bi-I bonds to μ iodides are similar in length with values of 3.32 Å and 3.33 Å and the terminal Bi-I bonds trans to the longest bonds are 2.97 Å and 2.92 Å, respectively (Figure 2a). The remaining bonds are close to the average bond length, with values of 3.03 Å and 3.09 Å. This geometry results in an octahedron with a lower value for Δ_{oct} (2.72×10^{-3}). However, the bond angles in this octahedron are more distorted, leading to a higher value of 8.03 for σ^2_{oct}. The value of λ_{oct} is similar to the other octahedron (0.985). In addition to intraoctahedral distortions, there is a degree of interoctahedral twisting along the Bi-Bi distance as measured using torsion angles. Torsion angles, in this case, are defined as the angle made between corresponding M-X bonds on adjacent octahedra (Figure S1). Note that this measurement is not purely caused by octahedral tilting with non-ideal octahedra but will also include contributions from intraoctahedral distortions. Therefore, we present average values of the 4 smallest torsion angles for neighboring octahedra to give an idea of the twisting along the Bi-Bi direction. There are two μ Bi-I-Bi bond angles in the structure with values of 178.40° and 160.40°. Along the latter bond angle, very little twisting is observed between the octahedra (average X-M-M-X torsion angle of 1.31°). The 178.40° μ Bi-I-Bi bond experiences more significant twisting, with an average X-M-M-X angle of 17.4° because of steric interactions between the organic cations and the terminal I anions.

The deviation in the 160.40° Bi-I-Bi bond angle from an ideal 180° is caused in part by interactions with the organic cations. There are two crystallographically unique TMPZ molecules in the structure of (TMPZ)BiI_5. The two cations are distinguished by their orientation relative to the propagation of the 1D Bi-I chains. Because the ammonium groups are quaternary, the cationic charge is born on the N-methyl and methylene groups that make close contacts with the iodide anions. Therefore, we will refer to these N-methyl groups to describe orientation of TMPZ. Additionally, because the central piperazine ring adopts a chair structure, we will distinguish the N-methyl moieties by the designation axial or equatorial (Figure S2). Note that the direction of the axial N-methyl group is always perpendicular to the nominal "plane" of the piperazine ring (Figure S2). Both TMPZ cations interact with two adjacent Bi-I chains, similar to dications in layered perovskite structures, resulting in the Bi-I chains stacking in an eclipsed fashion along the *b*-axis (Figure 1). These stacks then align along the *c*-axis with adjacent Bi-I chains offset along the *b*-axis by a Bi-I bond length. The equatorial N-methyl groups are closest to the μ-iodide anions (~3.5 Å for the closest H-I distance). When examining one Bi-I chain, there are 4 possible configurations for the axial N-methyl group closest to the chain (Figure 3): 1a) perpendicular to the direction of chain propagation (*a*-axis) and pointing away from the chain, 2a) the same as (1a) but pointing directly toward a terminal iodide, 3a) parallel to the *a*-axis and pointing at a terminal iodide, and 4a) antiparallel to (3a). Note that the orientations occur in pairs since (1a) and (4a) are related to (2a) and (3a), respectively, via translation from one side of a chain to the other side along the *b*-axis, flipping the orientation of the axial N-methyl closest to the chain 180° (Figure 3). In addition to these 4 interactions, there are additional interactions between the terminal iodides along the side

of a Bi-I chains with methylene hydrogen and axial N-methyl hydrogens of TMPZ cations in the adjacent stack of Bi-I chains. These interactions form close contacts (3.1-3.3 Å) with terminal iodides and are responsible for the offset between Bi-I chains in adjacent stacks.

The interaction between these 4 TMPZ orientations explain the interoctahedral distortions in (TMPZ)BiI_5. Each μ-I involved in a Bi-I-Bi bond angle that deviates greatly from 180° interacts with all 4 TMPZ molecules around it, working in concert to produce the distortion. Assigning each TMPZ cation a number based on the axial N-methyl group as described above, cations (1a) and (3a) both have equatorial N-methyl groups that point directly at the μ-I, causing a steric interaction that moves the iodide away from these moieties. This distortion is stabilized by close interactions (3.1 Å) with 4 hydrogens on methylene and axial N-methyl moieties from (2a) and (4a). Additionally, the axial N-methyl groups are pointed directly at terminal iodides *cis* to the μ-I, causing an additional steric interaction that favors the distorted Bi-I-Bi angle. The twisting of these two Bi-I octahedra for this non-ideal Bi-I-Bi bond angle is also responsible for the torsion observed along the nearly ideal Bi-I-Bi bond angle. Despite the structural distortions induced by the TMPZ cations, the bond lengths between bismuth and iodide ions remain relatively similar to distances observed in systems with less sterically bulky primary ammonium groups[32] and show only small deviations from the mean bond length (as reflected in the values of Δ_{oct} and λ_{oct}). For (TMPZ)BiI_5, the structure therefore has intact 1D Bi-I chains and the materials thermal properties are expected to reflect the extended nature of the structure. Therefore, we expect this material to behave more

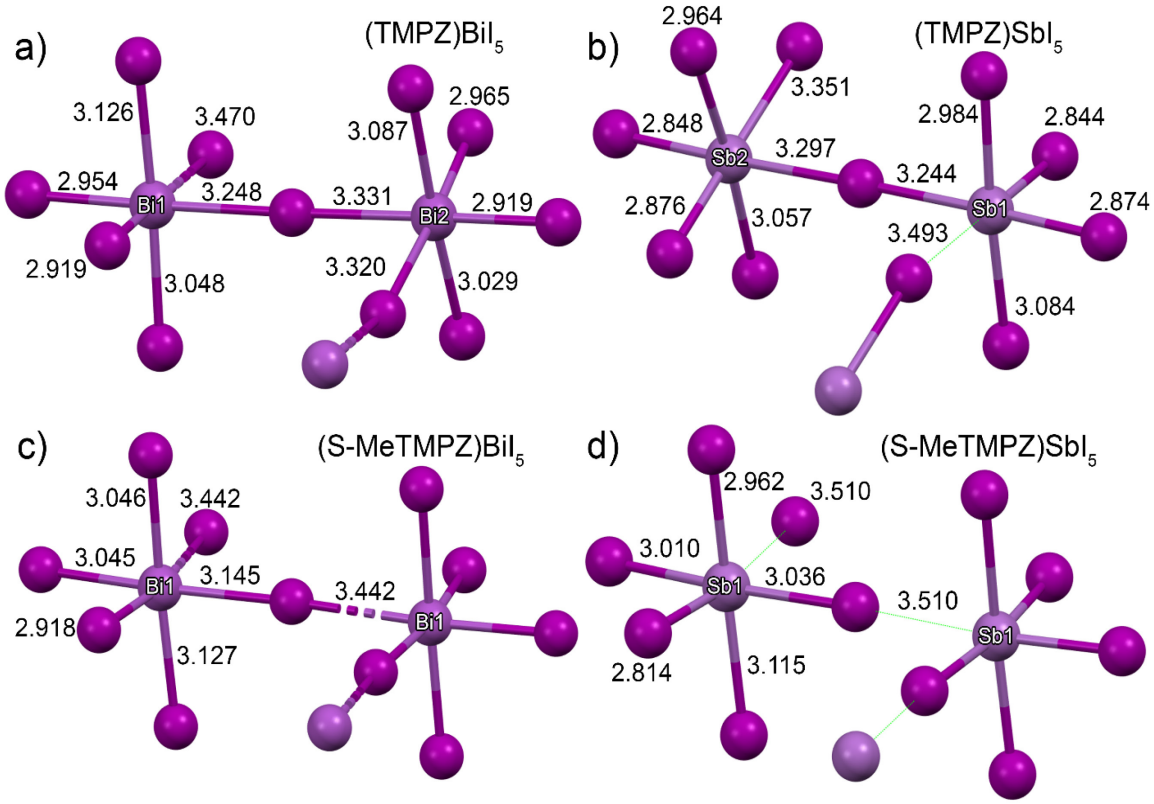

Figure 2. Comparison of bond lengths in fragments of the zig-zag 1D metal halide chains for: (a) (TMPZ)BiI_5, (b) (TMPZ)SbI_5, (c) (S-MeTMPZ)BiI_5, and (d) (S-MeTMPZ)SbI_5. Distances are shown in angstroms. The structure for (TMPZ)BiI_5 in panel (a) comes from ref 40.

like an extended solid like BiI_3 (which, however, is 2D versus 1D) rather than a molecular species

(for example SbI_3). If alteration of the organic cation or replacement of Bi^{3+} with Sb^{3+} could result in a lowering of the effective dimensionality to a structure that is more molecular in nature, we expect a lowering in the melting point of those structures. Therefore, we attempted to synthesize the unexplored antimony analog of (TMPZ)BiI_5 and replaced the organic cation with a bulkier chiral cation (S-MeTMPZ).

(TMPZ)SbI_5 is isostructural with (TMPZ)BiI_5 (i.e. *P-1* space group) except for a nominal 5.54 pm expansion along the *a*-axis (the direction of the 1D chain) and a 9.47 pm expansion along the *c*-axis (distance between layers of 1D chains) for the Sb analog. Accompanying the expansion along *a*- and *c*-axes, we observed a 7.01 pm reduction in the *b*-axis, which represents the distance between adjacent M-I chains. The inorganic chains in the antimony compound have the same basic structure as the bismuth analog. In general, the smaller ionic radius of Sb^{3+} results in Sb-I bonds (Figure 2b) that are shorter than the corresponding Bi-I bonds (Figure 2a), except for the longest M-I bond to the μ I, which is longer in the antimony compound at 3.49Å. This lengthened bond could be attributed to the increased structural activity of the stereoactive lone pair in antimony compared to bismuth compounds.[21] Additionally, the lengthening of this Sb-I distance suggests that this interaction represents a weaker covalent bond and a trend towards breaking up the extended chains into Sb-I dimers. The weakening of this bond by changing metals results in a decrease in the effective dimensionality of the structure, which we hypothesize leads to thermal properties tending more towards a molecular compound than to an extended 1D structure (i.e. a lower melting point is expected). The increased activity of the lone pair of Sb coupled with the reduction in Sb^{3+} size leads to changes in the distortion parameters of the two octahedra. The value of σ^2_{oct} is reduced in both octahedra from 7.58 and 8.03 for the Bi compound to 6.76 and 5.65, respectively, for the Sb compound. While the *cis* bond angles are closer to 90°, there is a greater degree of bond length distortion. The values for Δ_{oct} (5.33×10^{-3} and 4.06×10^{-3}) and λ_{oct} (1.01 and 1.03) are both increased significantly for (TMPZ)SbI_5 compared to the Bi compound, likely caused at least in part by the increased influence of the stereoactive lone pair. The increase in λ_{oct} does not as clearly demonstrate the increased distortion because the values are closer to 1 or only slightly further from 1 in the antimony compound compared to bismuth. However, the change from λ_{oct} values less than 1 in (TMPZ)BiI_5 to values greater than 1 in (TMPZ)SbI_5 shows the effect the

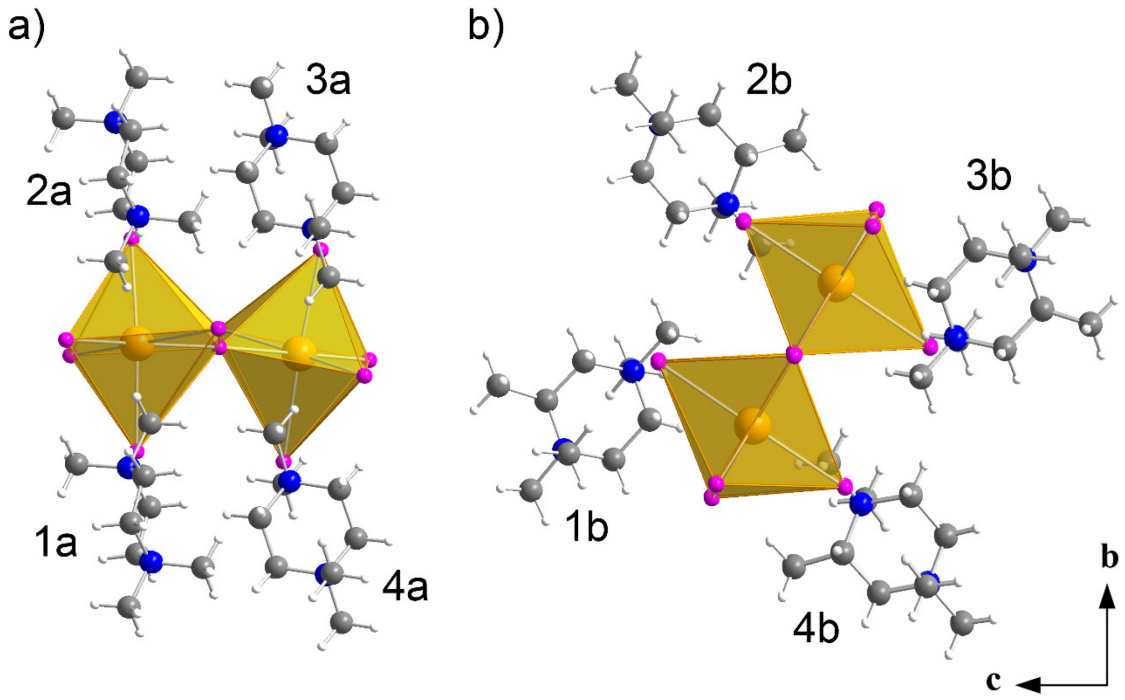

Figure 3. Diagram of organic molecule orientation relative to the Bi-I chains in (a) (TMPZ)BiI_5 and (b) (S-MeTMPZ)BiI_5. Unit cell axes for both compounds are shown in the bottom right.

longest bond length has on the range of bond lengths present in the structure and hints at the distortion observed when examining Δ_{oct}.

When TMPZ is replaced by S-MeTMPZ, the symmetry of the hybrid structure increases to the orthorhombic space group $P2_12_12_1$, resulting in only one crystallographically unique Sb and Bi octahedron in the structures. The relatively minor change in organic cation from TMPZ to S-MeTMPZ results in very different interactions between the organic cation and an individual M-I chain, as well as in the arrangement of the M-I chains relative to each other. The additional steric interactions introduced by adding an equatorial methyl group result in the organic cations orienting so that the chiral methyl groups point away from M-I chains. The S-MeTMPZ cations form stacks of "paired" cations along the *a*-axis, so that the chiral methyl groups of S-MeTMPZ are between the two stacks of cations (Figure 1). Relative to a single Bi-I chain, the interactions between S-MeTMPZ and the Bi-I chains are similar to the interactions within (TMPZ)BiI_5. There are 4 orientations (two mirrored pairs) of S-MeTMPZ, which place equatorial N-methyl moieties close to the μ-I anions, but in all cases an axial N-methyl group points at a terminal iodide (Figure 3b). Additionally, rather than the TMPZ cations rotating 90° so that the axial N-methyl groups change from parallel to the chain propagation to perpendicular, for S-MeTMPZ the molecules rotate approximately 90° so that the equatorial N-methyl groups change from parallel (1b and 3b) to perpendicular (2b and 4b) relative to the plane of the Bi cations in a single chain. In other words, when looking down the M-X chains, the long axis of the organic cation (Figure S2) is always normal to the plane of metal atoms in (TMPZ)MI_5, while for (S-MeTMPZ)MI_5 half of the organic cations have their long axis parallel to the metal atom plane. Also note that the S-MeTMPZ cations still bridge two Bi-I chains, but the equatorial N-methyl groups are parallel to the Bi plane in one and perpendicular in the other, resulting in the Bi-I chains being rotated relative to each other. There are two additional interactions at the edge of each Bi-I chain, with the terminal iodide anions

and the methylene and N-methyl groups of S-MeTMPZ cations closely associated with neighboring chains (close contacts approximate 3.1-3.3 Å).

The M=Bi and Sb (S-MeTMPZ)MI_5 hybrids (Figure 2c and 2d) are isostructural and the change from Bi to Sb has similar structural effects as those discussed for the (TMPZ)MI_5 hybrids. In both materials, there is only one unique octahedron, which has one long M-I bond length and, therefore, can be thought of as a square pyramid with a long contact between adjacent square pyramids. The lowering of effective dimensionality in both compounds is a result of the steric interactions of S-MeTMPZ with the inorganic chains. Because the S-MeTMPZ cations are inserted into the voids between the octahedra of the 1D chain and the bulky N-methyl groups are pointing directly to iodide anions in the chain (regardless of orientation), these steric interactions act to drive the 1D chain structure apart and result in a slightly more molecular structure. For (S-MeTMPZ)BiI_5, the longest Bi-I bond length is 3.44 Å and the shortest is 2.92 Å, similar to the values in (TMPZ)BiI_5 (Figure 2c). The other bond lengths range from 3.05-3.15 Å, with the longest being to the μ iodide anion. Changing the metal to Sb causes the longest bond length to increase to 3.51 Å (longest M-I bond length observed among any of the compounds considered) while all other bond lengths shrink (Figure 2d). This change is again ascribed to the stereoactive lone pair in Sb. The widening range of M-I bond lengths in (S-MeTMPZ)SbI_5 compared to (S-MeTMPZ)BiI_5 results in an increased value for Δ_{oct} of 4.89 x 10^{-3} versus 2.68 x 10^{-3} due to the stereoactive lone pair of Sb, driving the square pyramidal units further apart and causing one bond to deviate more from the average. Unlike the (TMPZ)MI_5 materials, (S-MeTMPZ)SbI_5 is less distorted overall than the Bi analog, as determined based on the λ_{oct} distortion parameter (1.02 vs 1.00). The (S-MeTMPZ)MI_5 materials show similarly high distortion of the *cis* I-M-I bond angles (σ^2_{oct} of 23.4 and 24.4 for Bi and Sb respectively) due to the inorganic chains distorting around the S-MeTMPZ cations, which penetrate the M-I chains. All of these distortions result in a more molecular structure, thereby suggesting that the (S-MeTMPZ)MI_5 compounds may have lower melting points than (TMPZ)MI_5 and that, of these, the Sb compounds may have lower melting points than the Bi analogs.

Thermal Properties

As stated earlier, from the limited set of compounds that we tested, melting was only observed with the quaternary ammonium compounds templated by TMPZ and S-MeTMPZ rather than primary alkylammonium-containing cations such as NEA and DDA. The first examples of meltable materials we discovered were (S-MeTMPZ)BiI_5 and (TMPZ)BiI_5, which melted on a hot plate heated to ~300 °C. The ground powders melt into black, shiny beads on the surface of glass substrates, suggesting that the resulting liquid is hydrophobic and has an unfavorable interaction with the hydrophilic glass surface. While the materials are melted, the liquids bubble and smoke (or vapor) evolves into the fume hood, suggesting that the materials partially decompose while in the molten state at the elevated temperature. On cooling, the materials harden into a brittle material that looks red when ground, like the original compounds before the melting experiment. Spurred on by these results, we prepared the antimony analogs (S-MeTMPZ)SbI_5 and (TMPZ)SbI_5, to try and lower the melting point of the materials, in analogy with the lower melting points observed in Sn 2D perovskite systems compared to Pb analogs.[13, 17-18, 43] An examination of isostructural Sb and Bi compounds would also help elucidate general melting trends, which cannot be deduced based on the isolated binary materials SbI_3 and BiI_3. Performing the same crude melting test, we found that these materials melt approximated 20 °C lower than the bismuth analogs, but similar

bubbling is observed for (TMPZ)SbI_5. While these qualitative assessments of melting demonstrate the ability to melt these materials, the melting point and decomposition of the materials required further study and quantification with thermogravimetric analysis (TGA) and differential scanning calorimetry (DSC).

The melting temperatures (T_m) and the melting enthalpies (ΔH_m) of the achiral and chiral set of compounds—i.e., (a) (TMPZ)BiI_5, (b) (TMPZ)SbI_5, (c) (S-MeTMPZ)BiI_5, and (d) (S-MeTMPZ)SbI_5—were extracted from the melting endotherms of phase pure ground crystals or precipitated powders (Figures S3-4) using DSC measurements (Figure 4, Figures S5-8, and Table S3). Notably, the achiral compounds have higher T_m than their chiral counterparts, (Figures S7-8 and Table S3) with the lowest T_m = 252.4 °C observed for (S-MeTMPZ)SbI_5. Such behavior has previously been seen in 2D chiral perovskites, wherein the asymmetric hydrogen bonding characteristics impart a lower T_m when compared to a more symmetric achiral structure.[12, 14] However, in these 1D systems, the quaternary ammonium cations cannot have well-defined directional hydrogen bonding interactions between the ammonium and the iodide anions. Instead, interactions between the N-methyl groups and iodides are expected to be weaker than hydrogen bonding with a primary ammonium group. The trend in melting point in these materials is better explained, at least in part, by the effective dimensional reduction caused by increased steric interactions in (S-MeTMPZ)MI_5 compared to (TMPZ)MI_5 compounds (discussed previously). Furthermore, due to higher lone pair stereochemical activity of Sb than Bi (i.e., further dimensional reduction), the T_m is reduced in the former by ~12 °C (Table S3), akin to the general observation in Pb, Sn, and Ge based perovskites, i.e., the T_m reduces while moving up along the metallic group in the periodic table.[21, 43]

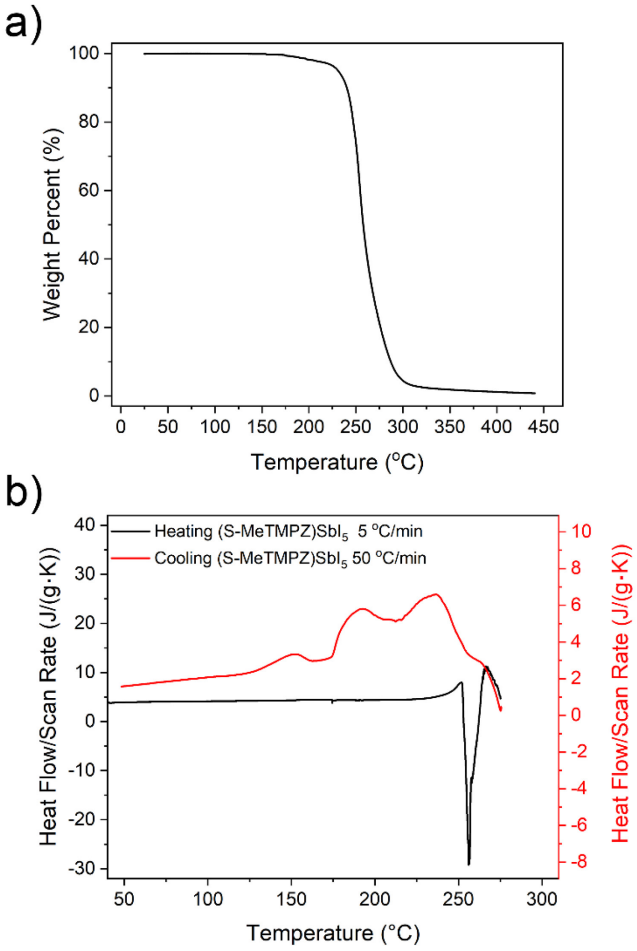

Figure 4. (a) TGA and (b) DSC scans of (S-MeTMPZ)SbI_5 powder, performed using 5 °C min^{-1} heating and ~50 °C min^{-1} cooling rates.

Though this is the first demonstration of melting in extended Bi or Sb-based perovskite-derived structures/materials, the deposition of melt-processed crystalline films was challenging under atmospheric pressure in the currently discussed systems, with the exception of (S-MeTMPZ)SbI_5. The DSC cooling curves obtained after melting of (TMPZ)MI_5 and (S-MeTMPZ)BiI_5 do not show any exothermic recrystallization features, revealing the inability of the associated melts to reorder during cooling (Figures S7-8). Such behavior likely results from

partial/complete decomposition of these systems under heating (given the bubbling observed from the melts on the glass slides, as described earlier).[22, 44-46] These Bi/Sb perovskites show a high degree of volatility at elevated temperatures, as investigated using thermogravimetric analysis (TGA). For (S-MeTMPZ)SbI_5, the measurement shows a 4.8% mass loss, prior to a bulk degradation onset temperature (T_d) of ~ 230 °C. Subsequently, the sample undergoes complete mass loss (reaching ~0% weight) at 310 °C (Figure 4). The higher end temperature (T_{end}, Table S3) required to generate the DSC melting endotherms for the first three compounds inadvertently decomposes the material (bulge in the DSC pan observed due to pressure buildup) and thereby prevents their reordering into the parent phase.[44-46] Interestingly, nominally complete recrystallization is observed on cooling of the (S-MeTMPZ)SbI_5 melt. Presumably, due to the reduced T_m, along with the sharp melting onset and narrow width (ΔT) of the melting endotherm (Figure S8 and Table S3), the material undergoes minimal decomposition. As a result, reordering can be achieved with full recovery of ΔH_m (Figure 4). Additionally, it is important to note that a direct comparison between the T_d and T_m for (S-MeTMPZ)SbI_5 is not entirely significant due to the kinetic nature of the former as opposed to the thermodynamic nature of the latter. T_d can thus vary depending on various factors, such as the particle size/form-factor of the sample, the heating rate, and the gas flow rate used in the TGA experiment. Moreover, it is worth mentioning that the DSC experiment used a hermetically sealed aluminum pan, in contrast to the open pan configuration used in TGA. This sealed configuration offers the potential for reorganization similar to melt-pressed film deposition under Kapton (discussed in the next section).

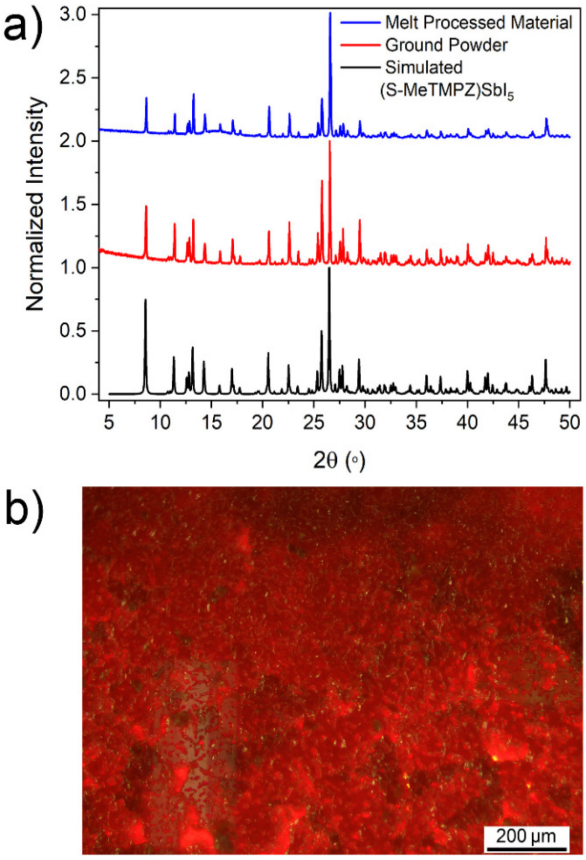

Figure 5. (a) PXRD and (b) optical microscope image of melt processed (S-MeTMPZ)SbI_5. The weak and broad diffraction feature centered at ~15° for the "melt-processed material" derives from the Kapton substrate. Simulated data derives from the single crystal structure of (S-MeTMPZ)SbI_5, assuming some preferential orientation along the (031) crystal plain with a March-Dollase parameter $r = 0.5$.

Melt Processing of Antimony Iodide Hybrids

Encouraged by the melt properties of the antimony-iodide-based materials, we then attempted to melt process powders of (TMPZ)SbI_5 and (S-MeTMPZ)SbI_5 to demonstrate the ability to crystallize the materials and to prepare films. We started experiments with (TMPZ)SbI_5. Given initial experiments on a hot plate, showing that the 1D pnictide-halide melts do not effectively wet a glass substrate, for the subsequent hot-pressing experiments we included Kapton as one of the substrates. Full details of the

pressing procedure can be found in the Supporting Information. Briefly, samples were loaded into a custom-built hot press (Figure S9)[47] after the top/bottom plates were heated to a temperature above the melting point of the material and were left in the press for a relatively short amount of time (a few seconds to one minute at most) to minimize material loss or degradation. The samples were then quenched while under pressure to facilitate recrystallization and to hinder organic cation loss.

Examination of the hot-pressed samples of (TMPZ)SbI_5 under a microscope shows that some of the material has visibly degraded, but relatively large hexagonal plate crystals similar in appearance to (TMPZ)SbI_5 also form; however, the majority phase within the film appears to be a lighter colored (yellow) decomposition-related phase (Figure S10). Correspondingly, powder X-ray diffraction (PXRD) analysis of the melted film shows that the main crystalline phase does not match the crystal structure of (TMPZ)SbI_5 (Figure S11). The PXRD data show a systematic shift of the most intense peaks to higher angle after melting, indicating a phase with a smaller d-spacing than the unmelted phase, coupled with new, intense diffraction peaks, which are not present in the simulated data for (TMPZ)SbI_5. Examining the data using a log scale reveals weak diffraction from the original (TMPZ)SbI_5 (Figure S11). The films were allowed to remain in the molten state for ~1 minute prior to cooling, and this extended time above T_m (and T_d) likely caused the observed degradation. Nevertheless, these results do point to the possibility of using the melt phase to grow and isolate crystals of the 1D perovskite phases, assuming degradation can be avoided by reducing the melting point or altering the processing method (i.e., better confining the melt or reducing the time at high temperature).

From earlier discussion, the most promising material for melt processing appears to be (S-MeTMPZ)SbI_5, due to it having the lowest melting point (T_m = 252.4 °C) and the ability to fully recrystallize from the melt (as seen in DSC data). Based on the experiences with (TMPZ)SbI_5, we also decided to lower the time the material remained in the melt state to further target improved film quality. Using this approach, we found that a few seconds exposure to the high temperatures was sufficient to melt the sample and prevent a large amount of material loss and decomposition. Therefore, experiments with (S-MeTMPZ)SbI_5 only remained at elevated temperature for 5 seconds before being quenched. An example of the resulting film is shown in Figures 5 and S12. For this material, large regions of the substrate are nominally uniformly covered with the dark red crystals of (S-MeTMPZ)SbI_5. Additionally, from PXRD analysis (Figure 5a), there are no obvious signs of an impurity phase, in contrast to the (TMPZ)SbI_5 films processed at higher temperature and for longer time. Film thickness using this melt-processing approach can be varied using applied pressure during the heating phase; the current films ranged in thickness from 2-5 μm. While the film results are encouraging and provide the first demonstration of successful melt processing of pnictide-based hybrid perovskites, further optimization is needed before the films can be employed for prospective devices. For example, the crystalline domains in the melt-processed films are quite small and the film surfaces are quite rough (Figures 5 and S12).

Conclusions

We have demonstrated for the first time that 1D pnictide-halide perovskites can be melted and, in one case, fully recrystallized from the melt into film form. Melting was confirmed in four compounds templated by TMPZ-related organic cations. Antimony-iodide-based materials have lower melting points than isostructural bismuth-iodide-based analogs. We attribute this difference, in part, to the lengthening of μ iodide to antimony bond lengths caused by the stereoactive lone

pair, coupled with an associated reduction in the effective dimensionality of the materials as TMPZ is replaced with the bulkier S-MeTMPZ. Overall, the melting points of these pnictide-iodide materials are higher than the 2D tin and lead compounds, likely due to the higher charge of the trivalent metals and increased ionic character of the materials. Despite the high melting point of these systems, we also show that (S-MeTMPZ)SbI_5 can be completely recrystallized after melt processing without introducing impurity phases. This further highlights the utility of exploring the thermal properties of pnictide-halides as well as the larger family of metal-halide hybrids (beyond the previously studied Ge, Sn and Pb based systems).

Acknowledgements

This research was financially supported by the Center for Hybrid Organic–Inorganic Semiconductors for Energy (CHOISE), an Energy Frontier Research Center funded by the Office of Basic Energy Sciences, Office of Science within the U.S. Department of Energy (synthetic and crystal structure analysis of compounds discussed), and by the NSF through grant number DMR-2114117 (thermal analysis and melting characterization of compounds discussed). B.C. carried out materials synthesis and film deposition studies as part of a Research Experience for Undergraduate (REU) students program supported by the National Science Foundation (award numbers 2050900, 2050841, and 2050764 and ECCS-2025064). All opinions expressed in this paper are the authors' and do not necessarily reflect the policies and views of the DOE or NSF. The authors thank Ken Gall for providing access to a differential scanning calorimetry tool for thermal analysis studies and Sasa Wang for assistance with the film thickness measurements.

Supporting Information

Electronic supplementary information (ESI) available: Experimental details, definition and calculation of intraoctahedral and interoctahedral distortion parameters, crystallographic data, and spectra are in the ESI. The CIFs for (S-MeTMPZ)SbI_5, (S-MeTMPZ)BiI_5, (TMPZ)SbI_5, and $(NEA)_3Bi_2I_9$ have been deposited in the CCDC under deposition numbers 2279626-2279629, respectively.

References

(1) Yan, C.; Huang, J.; Li, D.; Li, G., Recent progress of metal-halide perovskite-based tandem solar cells. *Materials Chemistry Frontiers* **2021,** *5* (12), 4538-4564.
(2) Kim, J. Y.; Lee, J. W.; Jung, H. S.; Shin, H.; Park, N. G., High-Efficiency Perovskite Solar Cells. *Chem Rev* **2020,** *120* (15), 7867-7918.
(3) Stranks, S. D.; Snaith, H. J., Metal-halide perovskites for photovoltaic and light-emitting devices. *Nat Nano* **2015,** *10* (5), 391-402.
(4) Smith, M. D.; Crace, E. J.; Jaffe, A.; Karunadasa, H. I., The Diversity of Layered Halide Perovskites. *Annu Rev Mater Res* **2018,** *48* (1), 111-136.
(5) Zou, C.; Zhang, C.; Kim, Y.-H.; Lin, L. Y.; Luther, J. M., The Path to Enlightenment: Progress and Opportunities in High Efficiency Halide Perovskite Light-Emitting Devices. *ACS Photonics* **2021,** *8* (2), 386-404.

(6) Zhang, T.; Wang, L.; Kong, L.; Zhang, C.; He, H.; Wei, B.; Yang, X., Halide perovskite based light-emitting diodes: a scaling up perspective. *J. Mater. Chem. C* **2021,** *9* (24), 7532-7538.
(7) Yang, T.; Li, F.; Zheng, R., Recent advances in radiation detection technologies enabled by metal-halide perovskites. *Materials Advances* **2021,** *2* (21), 6744-6767.
(8) Zhao, L.; Zhou, Y.; Shi, Z.; Ni, Z.; Wang, M.; Liu, Y.; Huang, J., High-yield growth of FACsPbBr3 single crystals with low defect density from mixed solvents for gamma-ray spectroscopy. *Nat. Photonics* **2023,** *17* (4), 315-323.
(9) Mitzi, D. B., Synthesis, Structure, and Properties of Organic-Inorganic Perovskites and Related Materials. In *Progress in Inorganic Chemistry*, John Wiley & Sons, Inc.: 2007; pp 1-121.
(10) Mao, L.; Stoumpos, C. C.; Kanatzidis, M. G., Two-Dimensional Hybrid Halide Perovskites: Principles and Promises. *J. Am. Chem. Soc.* **2018**.
(11) Dunlap-Shohl, W. A.; Zhou, Y.; Padture, N. P.; Mitzi, D. B., Synthetic Approaches for Halide Perovskite Thin Films. *Chem. Rev.* **2019,** *119* (5), 3193-3295.
(12) Singh, A.; Jana, M.; Mitzi, D. B., Organic-inorganic metal halide glass. US Patent App. 17/333,862: 2022.
(13) Mitzi, D. B.; Dimitrakopoulos, C. D.; Rosner, J.; Medeiros, D. R.; Xu, Z.; Noyan, C., Hybrid Field-Effect Transistor Based on a Low-Temperature Melt-Processed Channel Layer. *Advanced Materials* **2002,** *14* (23), 1772-1776.
(14) Singh, A.; Jana, M. K.; Mitzi, D. B., Reversible Crystal–Glass Transition in a Metal Halide Perovskite. *Advanced Materials* **2021,** *33* (3), 2005868.
(15) Salah, M. B. H.; Mercier, N.; Dabos-Seignon, S.; Botta, C., Solvent-Free Preparation and Moderate Congruent Melting Temperature of Layered Lead Iodide Perovskites for Thin-Film Formation. *Angew. Chem., Int. Ed.* **2022,** *61* (35), e202206665.
(16) Mayer, A.; Pourdavoud, N.; Doukkali, Z.; Brinkmann, K.; Rond, J.; Staabs, J.; Swertz, A.-C.; van gen Hassend, F.; Görrn, P.; Riedl, T.; Scheer, H.-C., Upgrading of methylammonium lead halide perovskite layers by thermal imprint. *Applied Physics A* **2021,** *127* (4), 237.
(17) Li, T.; Dunlap-Shohl, W. A.; Reinheimer, E. W.; Le Magueres, P.; Mitzi, D. B., Melting temperature suppression of layered hybrid lead halide perovskites via organic ammonium cation branching. *Chem. Sci.* **2019,** *10* (4), 1168-1175.
(18) Mitzi, D. B.; Medeiros, D. R.; DeHaven, P. W., Low-Temperature Melt Processing of Organic−Inorganic Hybrid Films. *Chem. Mater.* **2002,** *14* (7), 2839-2841.
(19) Li, T.; Zeidell, A. M.; Findik, G.; Dunlap-Shohl, W. A.; Euvrard, J.; Gundogdu, K.; Jurchescu, O. D.; Mitzi, D. B., Phase-Pure Hybrid Layered Lead Iodide Perovskite Films Based on a Two-Step Melt-Processing Approach. *Chem. Mater.* **2019,** *31* (11), 4267-4274.
(20) Li, T.; Dunlap-Shohl, W. A.; Han, Q.; Mitzi, D. B., Melt Processing of Hybrid Organic–Inorganic Lead Iodide Layered Perovskites. *Chem. Mater.* **2017,** *29* (15), 6200-6204.
(21) Mitzi, D. B., Synthesis, Crystal Structure, and Optical and Thermal Properties of $(C_4H_9NH_3)_2MI_4$ (M = Ge, Sn, Pb). *Chem. Mater.* **1996,** *8* (3), 791-800.
(22) Singh, A.; Mitzi, D. B., Crystallization Kinetics in a Glass-Forming Hybrid Metal Halide Perovskite. *ACS Materials Letters* **2022,** *4*, 1840-1847.
(23) Zhao, Y.; Zhao, J.; Guo, Y.; Zhao, J.; Feng, J.; Geng, Y.; Yang, J.; Gao, H.; Yuan, M.; Jiang, L.; Wu, Y., Reversible phase transition for switchable second harmonic generation in 2D perovskite microwires. *SmartMat* **2022,** *3* (4), 657-667.

(24) Pitaro, M.; Tekelenburg, E. K.; Shao, S.; Loi, M. A., Tin Halide Perovskites: From Fundamental Properties to Solar Cells. *Advanced Materials* **2022,** *34* (1), 2105844.
(25) Cao, J.; Yan, F., Recent progress in tin-based perovskite solar cells. *Energy & Environmental Science* **2021,** *14* (3), 1286-1325.
(26) Wolf, N. R.; Connor, B. A.; Slavney, A. H.; Karunadasa, H. I., Doubling the Stakes: The Promise of Halide Double Perovskites. *Angew. Chem., Int. Ed.* **2021,** *60* (30), 16264-16278.
(27) Slavney, A. H.; Hu, T.; Lindenberg, A. M.; Karunadasa, H. I., A Bismuth-Halide Double Perovskite with Long Carrier Recombination Lifetime for Photovoltaic Applications. *J. Am. Chem. Soc.* **2016,** *138* (7), 2138-2141.
(28) Mitzi, D. B., Organic−Inorganic Perovskites Containing Trivalent Metal Halide Layers: The Templating Influence of the Organic Cation Layer. *Inorg. Chem.* **2000,** *39* (26), 6107-6113.
(29) Khazaee, M.; Sardashti, K.; Sun, J.-P.; Zhou, H.; Clegg, C.; Hill, I. G.; Jones, J. L.; Lupascu, D. C.; Mitzi, D. B., A Versatile Thin-Film Deposition Method for Multidimensional Semiconducting Bismuth Halides. *Chem. Mater.* **2018,** *30* (10), 3538-3544.
(30) Ünlü, F.; Kulkarni, A.; Lê, K.; Bohr, C.; Bliesener, A.; Öz, S. D.; Jena, A. K.; Ando, Y.; Miyasaka, T.; Kirchartz, T.; Mathur, S., Single- or double A-site cations in $A_3Bi_2I_9$ bismuth perovskites: What is the suitable choice? *Journal of Materials Research* **2021,** *36* (9), 1794-1804.
(31) Saparov, B.; Hong, F.; Sun, J.-P.; Duan, H.-S.; Meng, W.; Cameron, S.; Hill, I. G.; Yan, Y.; Mitzi, D. B., Thin-Film Preparation and Characterization of $Cs_3Sb_2I_9$: A Lead-Free Layered Perovskite Semiconductor. *Chem. Mater.* **2015,** *27* (16), 5622-5632.
(32) Mitzi, D. B.; Brock, P., Structure and Optical Properties of Several Organic−Inorganic Hybrids Containing Corner-Sharing Chains of Bismuth Iodide Octahedra. *Inorg. Chem.* **2001,** *40* (9), 2096-2104.
(33) Mitzi, D. B., Templating and structural engineering in organic-inorganic perovskites. *J. Chem. Soc., Dalton Trans.* **2001,** (1), 1-12.
(34) Bi, W.; Louvain, N.; Mercier, N.; Luc, J.; Rau, I.; Kajzar, F.; Sahraoui, B., A Switchable NLO Organic-Inorganic Compound Based on Conformationally Chiral Disulfide Molecules and Bi(III)I_5 Iodobismuthate Networks. *Advanced Materials* **2008,** *20* (5), 1013-1017.
(35) Louvain, N.; Mercier, N.; Boucher, F., α- to β-(dmes)BiI5 (dmes = Dimethyl(2-ethylammonium)sulfonium Dication): Umbrella Reversal of Sulfonium in the Solid State and Short I···I Interchain Contacts—Crystal Structures, Optical Properties, and Theoretical Investigations of 1D Iodobismuthates. *Inorg. Chem.* **2009,** *48* (3), 879-888.
(36) Tao, K.; Li, Y.; Ji, C.; Liu, X.; Wu, Z.; Han, S.; Sun, Z.; Luo, J., A Lead-Free Hybrid Iodide with Quantitative Response to X-ray Radiation. *Chem. Mater.* **2019,** *31* (15), 5927-5932.
(37) Greenwood, N. N.; Earnshaw, A., *Chemistry of the Elements*. Second ed.; Elsevier Inc.: University of Leeds, U.K., 1997.
(38) Peresh, E. Y.; Sidei, V. I.; Zubaka, O. V.; Stercho, I. P., $K_2(Rb_2,Cs_2,Tl_2)TeBr_6(I_6)$ and $Rb_3(Cs_3)Sb_2(Bi_2)Br_9(I_9)$ perovskite compounds. *Inorganic Materials* **2011,** *47* (2), 208-212.
(39) Chang, J.-H.; Doert, T.; Ruck, M., Structural Variety of Defect Perovskite Variants $M_3E_2X_9$ (M = Rb, Tl, E = Bi, Sb, X = Br, I). *Z. Anorg. Allg. Chem.* **2016,** *642* (13), 736-748.
(40) Li, M. Q.; Hu, Y. Q.; Bi, L. Y.; Zhang, H. L.; Wang, Y. Y.; Zheng, Y. Z., Structure Tunable Organic Inorganic Bismuth Halides for an Enhanced Two-Dimensional Lead-Free Light-Harvesting Material. *Chem. Mater.* **2017,** *29* (13), 5463-5467.
(41) Lufaso, M. W.; Woodward, P. M., Jahn-Teller distortions, cation ordering and octahedral tilting in perovskites. *Acta Crystallogr., Sect. B* **2004,** *60* (1), 10-20.

(42) Robinson, K.; Gibbs, G. V.; Ribbe, P. H., Quadratic Elongation: A Quantitative Measure of Distortion in Coordination Polyhedra. *Science* **1971,** *172* (3983), 567-570.
(43) Singh, A.; Crace, E.; Xie, Y.; Mitzi, D. B., A two-dimensional lead-free hybrid perovskite semiconductor with reduced melting temperature. *Chem. Commun.* **2023,** *59* (53), 8302-8305.
(44) Shaw, B. K.; Hughes, A. R.; Ducamp, M.; Moss, S.; Debnath, A.; Sapnik, A. F.; Thorne, M. F.; McHugh, L. N.; Pugliese, A.; Keeble, D. S.; Chater, P.; Garcia, J. M. B.; Moya, X.; Saha, S. K.; A. Keen, D.; Coudert, F.-X.; Blanc, F.; Bennett, T. D., Melting of hybrid organic–inorganic perovskites. *Nature Chemistry* **2021,** *13* (8), 778–785.
(45) McHugh, L. N.; Thorne, M. F.; Chester, A. M.; Etter, M.; Užarević, K.; Bennett, T. D., Mechanochemically synthesised dicyanamide hybrid organic–inorganic perovskites, and their melt-quenched glasses. *Chem. Commun.* **2022,** *58* (24), 3949-3952.
(46) Shaw, B. K.; Castillo-Blas, C.; Thorne, M. F.; Gómez, M. L. R.; Forrest, T.; Lopez, M. D.; Chater, P. A.; McHugh, L. N.; Keen, D. A.; Bennett, T. D., Principles of melting in hybrid organic–inorganic perovskite and polymorphic ABX_3 structures. *Chem. Sci.* **2022,** *13* (7), 2033-2042.
(47) Dunlap-Shohl, W. A.; Li, T.; Mitzi, D. B., Interfacial Effects during Rapid Lamination within $MAPbI_3$ Thin Films and Solar Cells. *ACS Applied Energy Materials* **2019,** *2* (7), 5083-5093.

TOC Figure

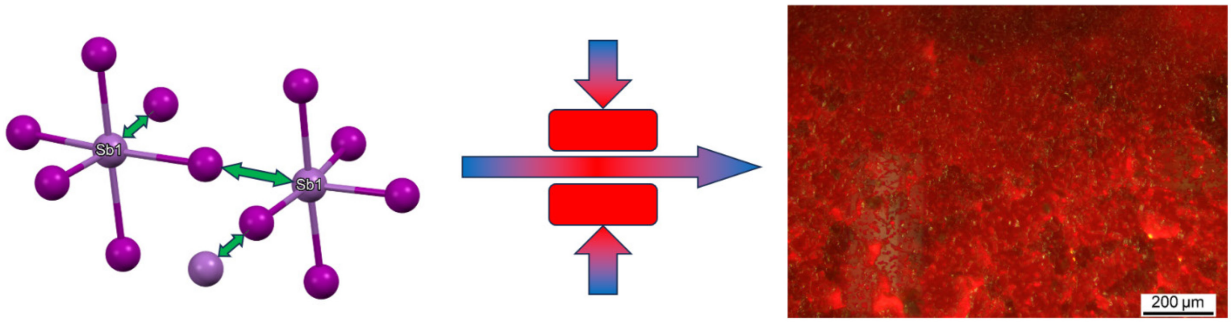

Synopsis

Various methods have allowed pnictide-based systems to capture properties of the hybrid lead-halide hybrid materials, but melt processing of such pnictide-halide materials has not been previously investigated. We demonstrate the ability to melt 1D hybrid pnictide-halide materials and develop a simple structure-property relationship to explain the observed trend in thermal properties. Finally, we fabricate melt-processed phase pure films of (S-MeTMPZ)SbI_5.